SPE 124689

Tracer Detection by Laser Spectroscopy for Applications in the Oil and Gas Industry

R. Nava, Texas A&M University, H. Schuessler, M. Fahes and H. Nasrabadi, Texas A&M University at Qatar, and A. Kolomenski, Texas A&M University

This paper was prepared for presentation at the 2009 SPE Annual Technical Conference and Exhibition held in New Orleans, Louisiana, USA, 4–7 October 2009.

Abstract

Tracer technology is very popular in petroleum engineering applications, and includes applications in reservoir characterization, reservoir modeling, improved oil recovery, etc. Most of the current tracer technology uses radioactive isotopes that are not environmentally friendly and require strict safety precautions. We propose the use of rare long-lived and stable noble gas isotopes as tracers, where instead of the decay of the radioactive material, we will use optical detection.

Due to their chemical inertness, rare noble gases offer the advantage that they do not react with the environment with which they are in contact. Our research employs for the first time optical detection of tracers by collinear fast beam laser spectroscopy. It has the additional advantage that novel tracer projects based on multiple tracers can be designed in the future.

In this work also the optical hyperfine structure of long lived ^{85}Kr was used to identify the ^{85}Kr tracer atoms. The technique has also been successfully applied to stable krypton isotopes. The abundance selectivity is at the one part in 10^{10} level and the sensitivity is at a few hundred ions. This method is several orders of magnitude more sensitive than the standard nuclear decay detection.
The new tracer technology offers a safer and more accurate option for applications in the oil and gas industry. The research work is currently being done in Qatar for application in Qatar's North Field.

Introduction

Tracer technology has very important applications in the oil and gas industry. Chemical or radioactive tracers are used to label fluids from specific locations in the reservoir, and trace them as they appear at other locations (Huseby et al., 2008). The results are used to evaluate inter-well connectivity and reservoir continuity, detect high permeability zones (Anisimov et al., 2009), identify residual oil saturation during waterflooding or miscible gas flooding applications (Devegowda et. al., 2009; Cockin et al., 2000), assess the success of fracture treatments (McDaniel et al., 2009), and many other applications such as precipitation in the near-wellbore region, and reservoir fluid sampling (Stamatakis et al, 2006; Gozalpour et al., 2005).

The application of tracers in the petroleum industry has been around for decades (Gore and Terry, 1956; Watkins and Mardock, 1954), and has proven to yield more accurate results on reservoir characterization than the use of pressure and rate data (Datta-Gupta et al., 1997; Huseby et al., 2009). Radioactive tracers such as Radon or natural tracers such as the ion-content of water are used to track injected fluids and identify the paths they traverse. However in most of the applications, the results yield qualitative evaluations rather than quantitative information about the reservoir.

The new tracer technology, which we are proposing for application in oil and gas reservoirs, has the advantage of a very high selectivity and sensitivity over traditional tracer technologies. The use of optical detection rather than radioactive decay or mass spectroscopy results in the ability of detecting about one tracer atom of ^{85}Kr in 10^{10} atoms in the natural background of ^{84}Kr. This is achieved using collinear fast ion beam laser spectroscopy detection. Rare noble gas isotopes are ideal candidates for such an application. In the next sections we review the technology of optical detection, discuss the

experimental setup and procedure for our work, and present some of the problems in the petroleum industry that can be addressed by applying this technology.

Theoretical Background

The collinear fast beam laser spectroscopy (CFBLS), introduced first by Kaufman (1976) and Wing et al. (1976) has evolved into a powerful tool of ultra-sensitive rare isotope detection (Iimura et al., 2003). It offers high sensitivity and selectivity due to several main features. First, mass separation of isotopes can be easily incorporated. Secondly, Doppler broadenings of the spectral lines can practically be eliminated by velocity bunching. An artificial isotope shift introduced in CFBLS by accelerating the ions to a large energy further separates the spectral lines of different isotopes. Finally, the ions are converted into neutral atoms by charge exchange collision readily allowing for the optical excitation of an atom beam in and around the visible region, which is much easier implemented, than the excitation necessary for ion beams requiring the UV spectral range.

The present work on krypton was motivated by the fact that ^{85}Kr is a major tracer gas for exploring the reservoir structure of large oil fields. ^{85}Kr detection in ambient air is also of importance for monitoring nuclear activities on a world wide scale (Otten, 1989). Our particle detection version of CFBLS combines small sample size with a high potential to be both an ultra-sensitive and ultra-selective detection scheme for ^{85}Kr . We obtain a high selectivity by sequential two step excitation with CW narrow band lasers to a suitably chosen Rydberg level, followed by field ionization. **Figure 1** displays the relevant energy levels of Kr for this scheme. In such a technique only signal ions, which have been resonant with two laser frequencies, are field ionized and detected. Such particle detection has obvious advantages over photon detection: the events can be detected with close to unity efficiency and the background of the scattered laser hght is eliminated. In addition, we use energy discrimination in an energy filter. This is possible, since the signal ions are produced with a characteristic energy, which is selectable by the field ionizer setting. The background ions produced as a result of collisions are to a large extent eliminated by the energy filter. Because of these advantages CFBLS has been the major technique for on-line and off-line laser spectroscopy of short-lived isotopes (Otten, 1989) as well as in trace isotope detection in samples taken from the environment, most notably for monitoring long-lived $^{89,90}Sr$ produced in nuclear fall out (Wendt et al., 1997).

Our theoretical analysis for the stepwise excitation is approximated by the three level atom model and summarized in **Figures 2** and **3**.

Experimental Setup and Procedure

The experimental setup is depicted in **Figure 4**. A hollow cathode discharge ion source (Danfysik 911A) generates a beam of Kr ions. The ions were extracted and accelerated to between 5 and 12 keV and mass-separated with a high transmission low-resolution bending magnet $(m/\Delta m \sim 230)$. The mass-selected ion beam is then deflected by a few degrees and co-propagates with laser beams from a Ti: Sapphire ring laser and a single-mode Ar^+ laser. The beam-line is evacuated by turbomolecular pumps to pressures below 10^{-6} torr. After passing through a post acceleration stage, the ion beam enters an alkali charge exchange cell for neutrahzation. In the near-resonant charge exchange reaction either cesium or rubidium vapors are used. A dominant fraction of the ions is thereby transferred into the metastable $5s^5[3/2]_2$ and $5s^5[1/2]_0$ levels. The remaining ions are deflected and the fast neutral metastable atoms enter the interaction region of about 0.8 meters in length. Thereafter the atoms pass through a collisional ionization cell or a field ionizer. In this way the Rydberg atoms can be either collisionally ionized or field ionized. The signal ions, after passing through a 135° energy filter, are detected with a Faraday cup or for low-level counting with a channeltron.

For the first excitation step a Ti: Sapphire ring laser (Coherent 899-21) pumped by an Ar^+ (Coherent Innova 200) is used. The linewidth of the actively-stabilized Ti: Sapphire laser is around 3 MHz. For the second-step excitation a single-frequency Ar^+laser (Coherent CR-2000K, operated at 488 nm wavelength) and equipped with a 1.0 cm fused silica solid state etalon is employed. This laser has a similar line-width of a few MHz. We monitor the single mode structure with a Burleigh 1.5 GHz scanning Fabry-Perot. A Burleigh wavemeter (resolution 0.01 cm^{-1}) helps to coarsely adjust the frequencies of the Ti: Sapphire laser. The two laser beams were combined using dichroic mirrors and directed collinearly into the fast beam apparatus.

The collisional ionization cell is made of a small gas chamber containing the collision gas. It has two apertures on either side of the walls. The chamber is encased in an outer cylindrical cell, which is differentially pumped by a turbomolecular pump (Leybold turbovac 361). The dependence of the collisional ionization cross-section with respect to different target gases has been investigated previously (Neugart et al., 1986; Borchers et al., 1989). For our collisional ionization cell with an effective cell length of 50 mm the best signals were obtained for collisional target gas pressures ranging from 40 mTorr to 100 mTorr.

Specifically, our scheme involves the following cascade excitations: $5s^2[3/2]_2 \rightarrow 5p^2[3/2]_1 \rightarrow 29d^2[7/2]_4$. Following the excitation, which is optimized by the laser power, atoms in the $29d^2[7/2]_4$ level are field ionized. With the ion counting of the hyperfine structure resonances of ^{85}Kr , providing a unique fingerprint, the minute quantities of this isotope are detected.

Collisional ionization detection proved very helpful in tuning and maximizing the two sequential laser excitation steps. It was important to tune the recyclable transition transition at 811.5nm. **Figure 5-a** shows the "flop in" signal observed in this case. For other not interesting first excitation steps "flop out" signals like depicted in **Figure 5-b** were recorded. In such a case the atoms are lost, since they can decay back to the ground state.

An important prerequisite for reaching high detection sensitivity was to optimize the charge exchange ratio. **Figure 6** demonstrates that when using Rubidium in the charge exchange cell 80% neutralization yields about 80% detection efficiency (8 on a scale of 10 in **Figure 6**).

For the initial observation of the hfs splittings of the various transitions a natural krypton sample slightly enriched with ^{85}Kr was prepared. The ^{85}Kr concentration was about 10^{-6}. With it the first excitation step from the $5s^2[3/2]_2 \rightarrow 5p^2[5/2]_3$ was readily detected using collisional ionization only. It is noted that such a signal can only be observed with an enriched sample, since otherwise the resolution of the one-step excitation is not sufficient to suppress the background from the neighboring ^{85}Kr isotope even though mass separation was used. After the hfs of ^{85}Kr had been determined in this way, we employed a more dilute sample produced at the TAMU reactor with a ^{85}Kr concentration of 10^{-8}. The ^{85}Kr concentration for this sample and subsequent ones obtained by dilution were determined by low level β-counting, and alternatively also from the measured ratio of the ^{85}Kr to ^{84}Kr signals observed with the complete cascade two-step excitation field ionization method. **Figure 7** compiles ^{85}Kr concentration measurement from various samples. Typical results for the recyclable hfs transition of ^{85}Kr with different sample concentrations show reasonable agreement, with the CFBLS optical measurement being consistently lower by about a factor of two. Further dilutions established our presently best value for the selectively of about 1×10^{10} and the sensitivity of a few hundred ^{85}Kr atoms/s.

Proposed Applications in the Oil and Gas Industry

Qatar's North field is the largest known non-associated gas field in the world (approximately 20% of the world's known gas reserves). The reservoir consists of four producing layers from the Khuff formation (K1, K2, K3 and K4). The field produces from a carbonate gas-condensate reservoir with a Condensate-Gas-Ratio (CGR) of about 40 STB/MMSCF. The reservoir initial pressure (5315 psi) is close to the dew point pressure (5135 psi) indicating that condensate dropout occurs since the reservoir is being produced below dew point (Whitson et al., 2005). The proposed tracer technology can be applied to tackle many of the problems and answer some of the questions that the petroleum industry in Qatar faces. Some of these problems are the following:

1. Calculating the contribution of each layer in producing commingled wells. This can be achieved by analyzing fluid samples from each layer and identifying natural tracers or tracers injected into these layers at other well locations. The results can also be used to detect problems that might be associated with formation damage in some of the layers. This may include the analysis of condensate dropout.
2. Studying the connectivity of various blocks. There are indications of compositional variation in the North Field, and although this can be the result of different source rocks, biodegradation, diffusion or other physical phenomena, it could also be due to low-permeability barriers. Studying the connectivity of various wells, the locations of barriers and of high permeability streaks is very important for better development of this important hydrocarbon resource.
3. Detecting leaks from the gas fields by analyzing air samples. Measuring tracer gas content in air samples taken from various locations can lead to a better understanding of the reservoir in terms of its sealing capability. The high selectivity and sensitivity of this method makes it a great candidate for such an application.
4. Improving fluid sampling procedures. When tracers are added to the drilling fluid, it will be easier to detect any infiltration to the fluid sample.

Although current tracer technology could address these issues, the proposed technology results in much more accurate results and is surely safer than the application of radioactive tracers. Our work will continue towards the application of this technology in Qatar. We are in the process instituting a tracer laboratory by putting together this experimental setup in Qatar and acquiring gas samples from Qatar's North Field for testing.

Conclusions

In this paper, we present a summary of the work that was conducted in order to develop the application of collinear fast ion beam laser technology in Qatar. Current tracer applications in the oil and gas industry will benefit from added accuracy , safety, and simultaneousmultipletracer methods associated with this new technology. The method of optical detection develloped here is orders of magnitude more accurate than conventional tracer detection methods. It has abundance selectivity at the one part in 10^{10} level at mass 85amu and the sensitivity is at a few hundred ions.

Acknowledgements

This research is supported by the Welch Foundation, grant A-1546, the National Science Foundation under grant No.0722800 and the Qatar National Research Fund, grant NPRP30-6-7-35.

References

Anisimov, L. A., Kilyakov, V. N., and Vorontsova, I. V.: "The Use of Tracers for Reservoir Characterization". SPE paper 118862. SPE Middle East Oil & Gas Show and Conference, Bahrain, 15-18 March, 2009.

Borchers, W., Arnold, E., Neu, W., Neugart, R., Wendt, K., Ulm, G., and ISOLDE Corporation, *Phys. Lett.* B 216, 7 (1989)

Cockin, A. P., Malcolm, L. T., McGuire, P. L., Giordano, R. M., and Sitz, C. D.: "Analysis of a Single-Well Chemical Tracer Test to Measure the Residual Oil Saturation to a Hydrocarbon Miscible Gas Flood at Prudhoe Bay". *SPE Reservoir Evaluation and Engineering*. (December 2000) 544-551.

Datta-Gupta, A., Vasco, D. W., and Long, J. C. S.: "On the Sensitivity and Spatial Resolution of Transient Pressure and Tracer Data for Heterogeneity Characterization". *SPE Formation Evaluation*. (June 1997) 137-144.

Devegowda, D., Akella, S., Datta-Gupta, A., and Efendiev, Y.: "Interpretation of Partitioning Interwell Tracer Tests Using EnKF With Coarse-Scale Constraints". SPE paper 119125. SPE Reservpor Simulation Syposium, The Woodlands, Texas, USA, 2-4 February, 2009.

Gore, G. L. and Terry, L. L.: "Radioactive Tracer Techniques". *Journal of Petroleum Technology*. (September 1956) 12-17.

Gozalpour, F., Danesh, A., Todd, A. C., and Tohidi, B.: "Application of Tracers in Oil-Based Mud for Obtaining High-Quality Fluid Composition in Lean Gas-Condensate Reservoirs". *SPE Reservoir Evaluation and Engineering*. (February 2007) 5-11.

Huseby, O., Valestrand, R., Nævdal,G., and Sagen, J.: "Natural and Conventional Tracers for Improving Reservoir Models Using the EnKF Approach". SPE paper 121190. SPE EUROPEC/EAGE Annual Conferenec and Exhibition, Amsterdam, The Netherlands, 8-11 June, 2009.

Huseby, O., Andersen, M., Svorstøl, I., and Dugstad, Ø.: "Improved Understanding of Reservoir Fluid Dynamics in the North Sea Snorre Field by Combining Tracers, 4D seismic, and Production Data". *SPE Reservoir Evaluation and Engineering*. (August 2008) 768-777.

Kaufman, S. L., *Opt. Commun*. **17**, 309 (1976).

McDaniel, R. R., Holmes, D. V., Borges, J. F., Bajoie, B. J., Peeples, C. R., and Gardner, R. P.: "Determining Propped Fracture Width From a New Tracer Technology". SPE paper 119545. SPE Hydraulic Fracturing Technology Conference, The Woodlands, Texas, USA, 19-21 January, 2009.

Neugart, R., Klempt, W., and Wendt, K., *Nuc. Instrum. Methods* **B17**, 354-359 (1986)

Otten, E. W., in *Treatise on heavy ion science*, **8**, 517 Plenum Press (London) (1989)

Stamatakis, E., Haugan, A., Chatzichristos, C., Stubos, A., Muller, J., Dugstad, Ø., and Palyvos, I.: "Study of Calcium Carbonate Precipitation in the Near-Well Region Using ^{47}Ca as Tracer". *SPE Production and Operations.* (February 2006) 33-39.

Watkins, J. W. and Mardock, E. S.: "Use of Radioactive Iodine as a Tracer in Water-Flooding Operations". *Petroleum Transactions, AIME*. (September 1954). 117-124.

Wendt, K., Bhowmick, G. K., Bushaw, B. A., Herrmann, G., Kratz, J. V., Lantzsch, J., Müller, P., Nörtershäuser, W., Otten, E.-W., Schwalbach, R., Seibert, W.-A., Trautmann, N., and Waldek, A., *Radiochimica Acta* **79**, 183 (1997)

Whitson, C. H. and Kuntadi, A.: "Khuff Gas Condensate Development". SPE paper 10692. International Petroleum Technology Conference, Doha, Qatar, 21-23 November, 2005.

Wing, W. H., Ruff, G. A., Lamb, W. E., and Spezeski, J. J., *Phys. Rev. Lett.* **36**, 1488 (1976).

Figures

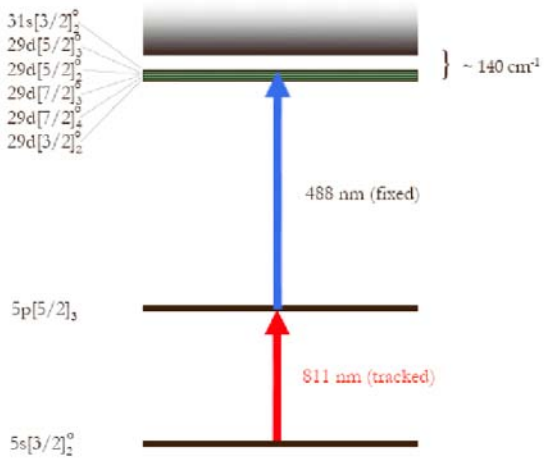

Figure 1 – The excitation scheme (Beam energy 5-12ev)

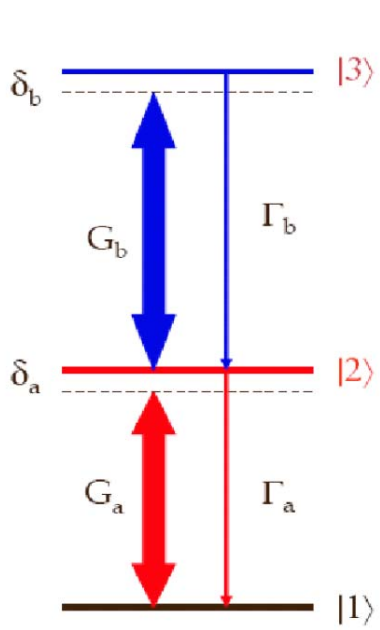

The QED rate equation[6]:

$$\langle \dot{\chi}_{11} \rangle = iG_a\langle \chi_{21}\rangle - iG_a^*\langle \chi_{12}\rangle + 2\Gamma_a\langle \chi_{22}\rangle$$

$$\langle \dot{\chi}_{22} \rangle = 2\Gamma_b\langle \chi_{33}\rangle + iG_b\langle \chi_{32}\rangle - iG_a\langle \chi_{21}\rangle + iG_a^*\langle \chi_{12}\rangle - iG_b^*\langle \chi_{23}\rangle - 2\Gamma_a\langle \chi_{22}\rangle$$

$$\langle \dot{\chi}_{33} \rangle = -2\Gamma_b\langle \chi_{33}\rangle - iG_b\langle \chi_{32}\rangle + iG_b^*\langle \chi_{23}\rangle$$

$$\langle \dot{\chi}_{32} \rangle = -iG_b^*\langle \chi_{33}\rangle + (i\delta_b - \Gamma_a - \Gamma_b)\langle \chi_{32}\rangle - iG_a\langle \chi_{31}\rangle + iG_b^*\langle \chi_{22}\rangle$$

$$\langle \dot{\chi}_{23} \rangle = iG_b\langle \chi_{33}\rangle + (-i\delta_b - \Gamma_a - \Gamma_b)\langle \chi_{23}\rangle + iG_a^*\langle \chi_{13}\rangle - iG_b\langle \chi_{22}\rangle$$

$$\langle \dot{\chi}_{31} \rangle = -iG_a^*\langle \chi_{32}\rangle + (i\delta_a + i\delta_b - \Gamma_b)\langle \chi_{31}\rangle + iG_b^*\langle \chi_{21}\rangle$$

$$\langle \dot{\chi}_{13} \rangle = -iG_b\langle \chi_{12}\rangle - (i\delta_a + i\delta_b + \Gamma_b)\langle \chi_{13}\rangle + iG_a\langle \chi_{23}\rangle$$

$$\langle \dot{\chi}_{21} \rangle = iG_b\langle \chi_{31}\rangle + (i\delta_a - \Gamma_a)\langle \chi_{21}\rangle + iG_a^*\langle \chi_{11}\rangle - iG_a^*\langle \chi_{22}\rangle$$

$$\langle \dot{\chi}_{12} \rangle = -iG_b^*\langle \chi_{13}\rangle - (i\delta_a + \Gamma_a)\langle \chi_{12}\rangle - iG_a\langle \chi_{11}\rangle + iG_a\langle \chi_{22}\rangle$$

Figure 2 – Level population and atomic coherences for a three-level atom interacting with two laser fields.

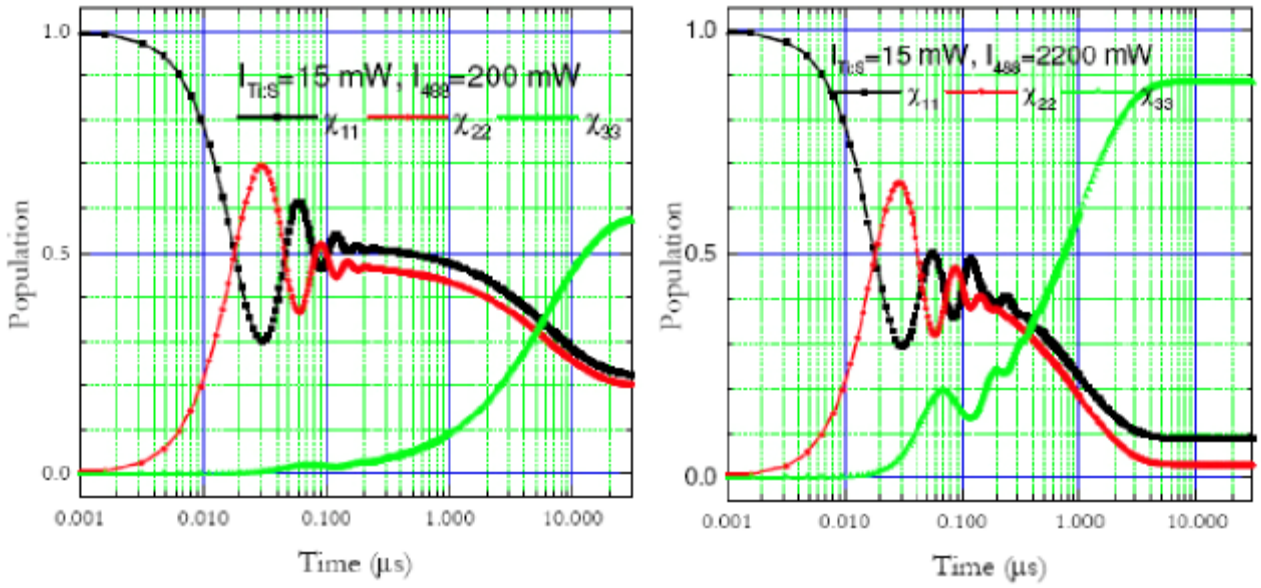

Figure 3 – Calculated population dynamics at different Ar^+ powers

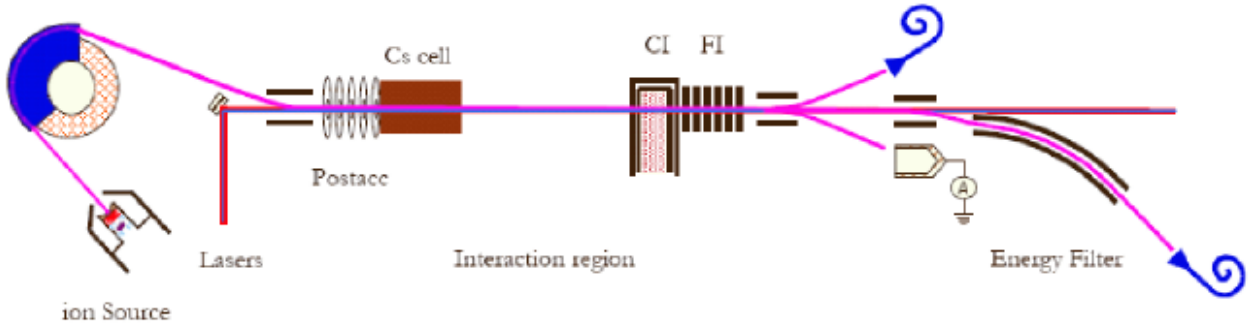

Figure 4 – Experimental Setup

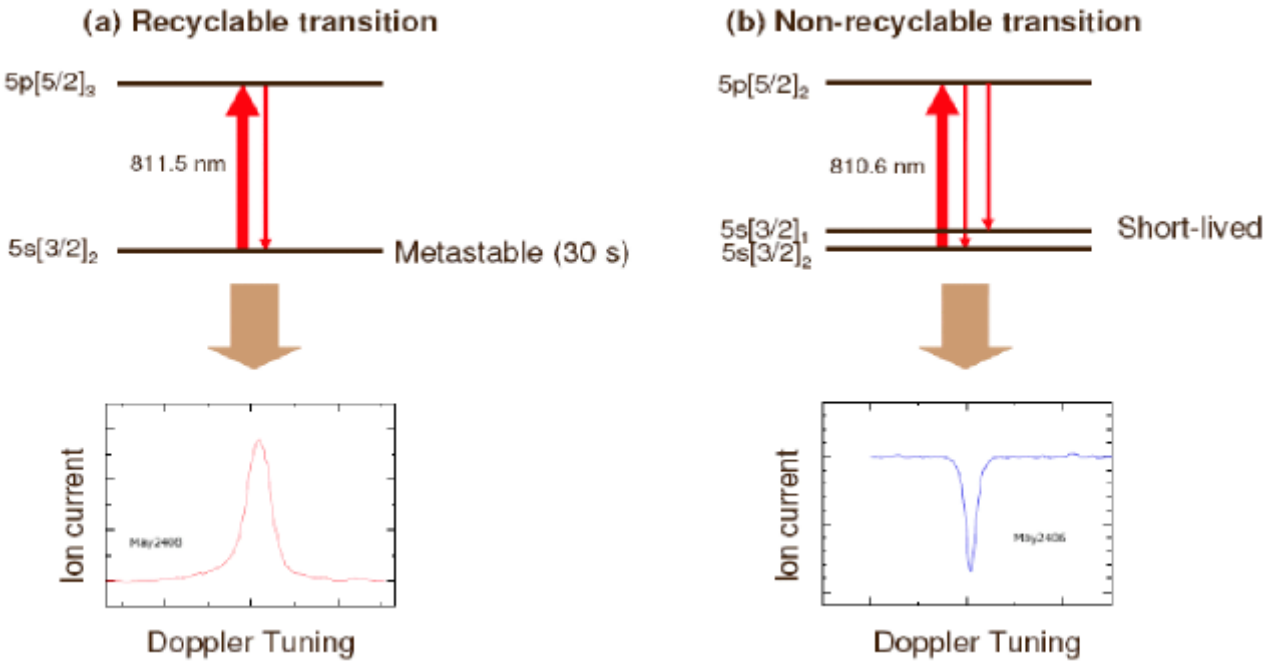

Figure 5 – Detection of Kr optical transitions by collisional ionization.

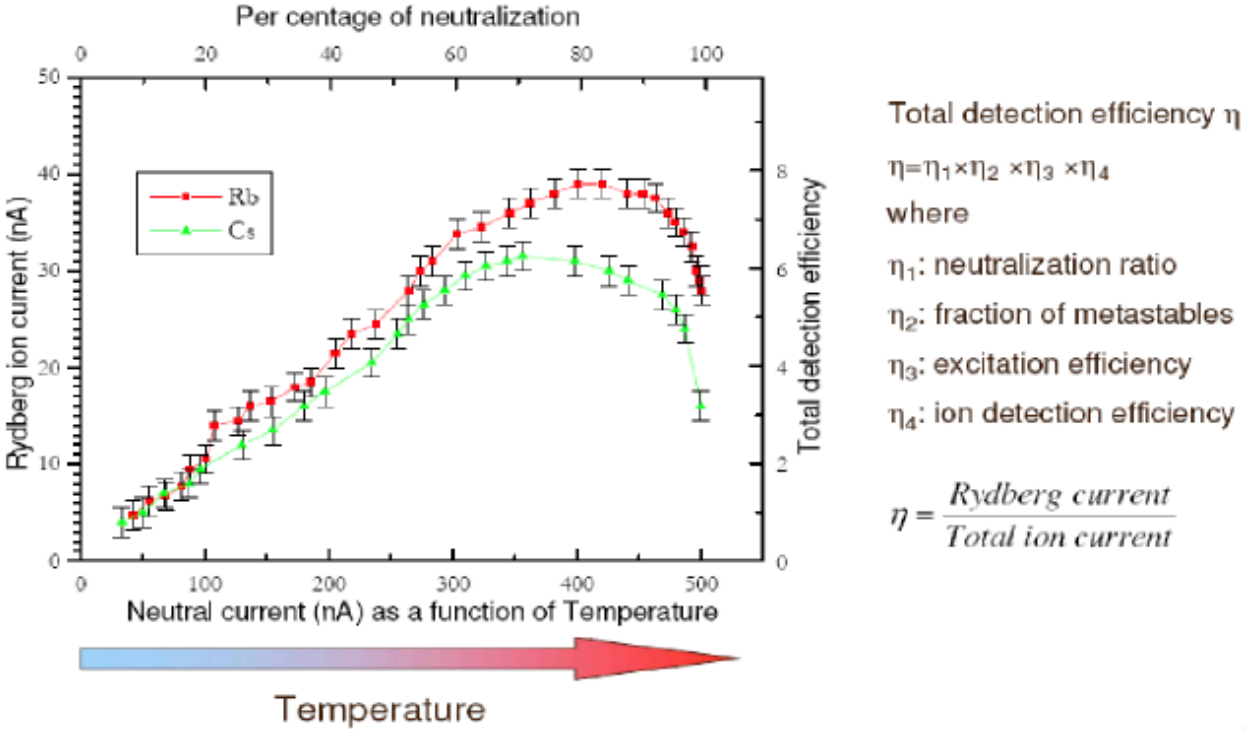

Figure 6 – Detection efficiency vs. neutralization ratio and charge exchange media.

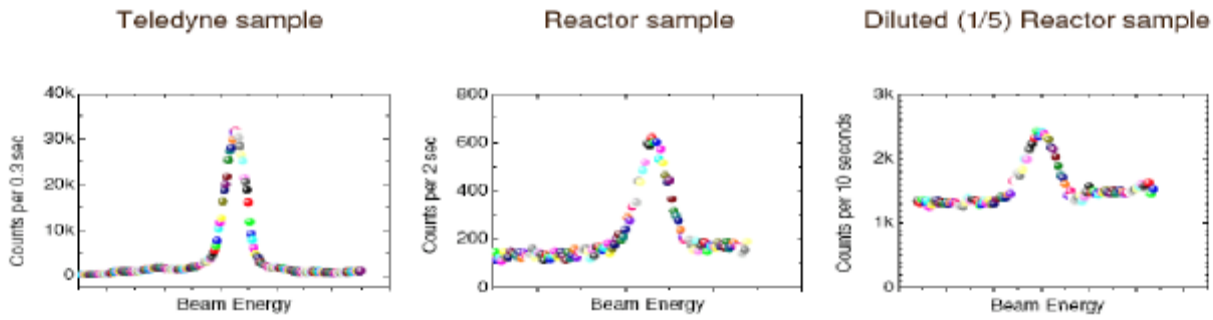

Sample	Teledyne	Reactor	Diluted Reactor
Expt.	4.0E-6	9.3E-9	1.8E-9
From activity Measurements	1.9E-6	1.6E-8	3.2E-9

Figure 7 – Results of concentration measurements in various samples.